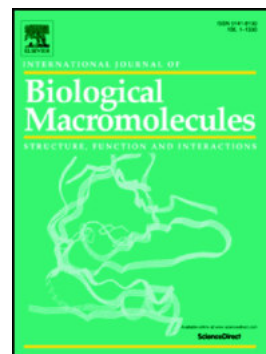


Accepted Manuscript

Green one-step synthesis of ZnO/cellulose nanocrystal hybrids with modulated morphologies and superfast absorption of cationic dyes

Ying Guan, Hou-Yong Yu, Somia Yassin Hussain Abdalkarim, Chuang Wang, Feng Tang, Jaromir Marek, Wei-Lai Chen, Jiri Militky, Ju-Ming Yao



PII: S0141-8130(18)37287-8

DOI: <https://doi.org/10.1016/j.ijbiomac.2019.03.104>

Reference: BIOMAC 11934

To appear in: *International Journal of Biological Macromolecules*

Received date: 26 December 2018

Revised date: 23 February 2019

Accepted date: 17 March 2019

Please cite this article as: Y. Guan, H.-Y. Yu, S.Y.H. Abdalkarim, et al., Green one-step synthesis of ZnO/cellulose nanocrystal hybrids with modulated morphologies and superfast absorption of cationic dyes, *International Journal of Biological Macromolecules*, <https://doi.org/10.1016/j.ijbiomac.2019.03.104>

This is a PDF file of an unedited manuscript that has been accepted for publication. As a service to our customers we are providing this early version of the manuscript. The manuscript will undergo copyediting, typesetting, and review of the resulting proof before it is published in its final form. Please note that during the production process errors may be discovered which could affect the content, and all legal disclaimers that apply to the journal pertain.

Green one-step synthesis of ZnO/cellulose nanocrystal hybrids with modulated morphologies and superfast absorption of cationic dyes

Ying Guan^{a,c}, Hou-Yong Yu^{a*,b}, Somia Yassin Hussain Abdalkarim^a, Chuang Wang^a,
Feng Tang^a, Jaromir Marek^d, Wei-Lai Chen^a, Jiri Militky^d, Ju-Ming Yao^{a*}

^aThe Key Laboratory of Advanced Textile Materials and Manufacturing Technology of Ministry of Education, College of Materials and Textile, Zhejiang Sci-Tech University, Hangzhou 310018, China

^b State Key Laboratory for Modification of Chemical Fibers and Polymer Materials, College of Materials Science and Engineering, Donghua University, Shanghai 201620, China

^c Zhejiang Provincial Key Laboratory of Chemical Utilization of Forestry Biomass, Zhejiang A&F University, Hangzhou 311300, China.

^dInstitute for Nanomaterials, Advanced Technologies And Innovations, Studentska 1402/2, Liberec, Czech Republic.

Abstract

Zinc oxide/cellulose nanocrystal (ZnO/CNC) hybrids with modulated morphologies were prepared by using bamboo CNC as templates via green one-step technique. The effect of pH values on the morphology, microstructure, thermal stability, antibacterial efficiency and dye absorption kinetics of hybrids were investigated. A possible

^{a*}Corresponding author. Tel.: 86 571 86843618; fax: 86 571 86843619.

E-mail addresses: phdyu@zstu.edu.cn (Hou-Yong Yu); yaoj@zstu.edu.cn (Ju-Ming Yao)

mechanism for various hybrid morphologies at different pH values was provided. All the samples exhibited high antibacterial ratios of 91.4%-99.8% against both *Escherichia coli* and *Staphylococcus aureus*. ZnO/CNC8.5 gave quick removal efficiency with high dye removal ratios in methylene blue (MB, 93.55%) and malachite green (MG, 99.02%), especially more than 91.47% and 97.85% within 5 minutes. The absorption capacity could reach up to 46.77 mg/g for MB and 49.51 mg/g for MG. Besides, absorption kinetics showed that the absorption behavior followed the pseudo-second-order kinetic model ($R^2 > 0.99996$). Such ZnO/CNC hybrids show outstanding and low-cost adsorbent for efficient absorption of cationic dyes in wastewater treatment field.

Keywords: ZnO/cellulose nanocrystal hybrids; Morphological modulation; Cationic dye absorption

1. Introduction

In the past decade, zinc oxide/cellulose nanocrystal (ZnO/CNC) hybrids are well-known as a fast-developing functional material in the interdisciplinary fields due to their prominent applications in photocatalysts, antimicrobial products, sensor, medical dressings, food packaging and sustainable functional materials [1-6]. As a renewable raw material, biodegradable and non-toxic CNC possesses some attractive characteristics, such as large specific surface area, high aspect ratio, superior mechanical strength, and so on. In general, dispersion and compatibility can be identified as two grand challenges for CNC before their uses in new functional materials. Additionally, CNC is thought to be less reactive when compared to amorphous cellulose

chains and the uses of only CNC as functional nanomaterials have shown some drawbacks arising from low antibacterial activity, stability against moisture and ultraviolet (UV) permeability, which can restrict their applications [7]. However, the hydroxyl groups on CNC surface provide reactive platforms for chemical modifications and introduction of additional functional groups. Moreover, in order to furnish and exploit the new functionalities of CNC, ZnO nanoparticles have been incorporated into CNC products. Recently, ZnO/CNC hybrids have been proposed [3, 6, 8, 9]. Compared to available metal nanoparticles, ZnO nanoparticles with relatively cheap cost have non-toxic nature, excellently antibacterial, electrical, photocatalytic, optical performance and various morphologies [10]. All the above performances make ZnO nanoparticles a good choice for the modification of CNC. Unfortunately, since the size of the ZnO nanoparticles is small, the surface free energy is high, and thus nanoparticles are easily agglomerated. The key to the successful preparation of the well-dispersed ZnO nanoparticles is to select suitable templates or process conditions [11]. The hybrid combination of CNC as templates with ZnO nanoparticles has become attractive, the attempts not only achieve prospect of modifying and functionalizing cellulose nanocrystals but also overcome the aggregation of ZnO nanoparticles. Therefore, more attempts have been undertaken on the synthesis of ZnO/CNC hybrids. A variety of fabrication/hybridization techniques have been used for the synthesis of ZnO/CNC hybrids, such as precipitation method, in situ solution casting technique and hydrothermal method [12-14]. CNCs using as template were from different cellulose sources. Experimental time, temperature, CNC concentration, weight/mass ratio and pH

value were changed to modulate the shape and size of ZnO nanoparticles. So far, few publications have reported on the preparation of different morphologies of ZnO/CNC nanohybrids by various fabrication methods. Typical morphologies, mechanism for shape/size and applications of ZnO/CNC hybrids obtained by a variety of methodologies are summarized in Table 1. Little works for using bamboo cellulose nanocrystal as template in modulating ZnO/CNC morphologies at different pH values were reported.

In our previous reports (Table 1), CNC was extracted from viscose acetal fibers in a hydrothermal reaction kettle at 110 °C and carboxyl groups were introduced on CNC surface. Flower-like ZnO/CNC hybrids were successfully prepared by precipitation method at 110 °C in oil bath as well as 97.35% of MB dye was decomposed with hybrids after 8 h [13]. Carboxyl groups were introduced on CNC surface and the products demonstrated promising antimicrobial activity for *Staphylococcus aureus* (*S. aureus*) and *Escherichia coli* (*E. coli*). Besides, Azizi et al. reported that the CNC was prepared by sulfuric acid hydrolysis, and ZnO/CNC nanocomposites with irregular hexagonal shapes were synthesized in organic solvents at 80 °C and yielded effective antimicrobial activity [9]. However, the introduction of charged sulfate groups on the CNC surface compromised the thermostability of the ZnO/CNC nanocomposites. The onsets of thermal degradation of three samples were found below 230 °C. The above methods exhibited not only higher reaction temperatures but also some organic solvents, which were not efficient and eco-friendly for their commercialization in industrial applications. Longer degradation time of dye was needed and lower thermal degradation

temperature was found for ZnO/CNC hybrids. The morphology was lack of diversity for the products. Generally, the unique performance properties of ZnO/CNC hybrids were dependent on their morphologies [15-17]. Therefore, there is still a challenge to develop a simple and environmentally friendly method using solely water in mild conditions to fabricate ZnO/CNC hybrids with multiple morphologies, effective antibacterial property and better absorption properties for wastewater treatment. One-step synthesis technique in this work has generated a great deal of interest in terms of green synthesis, facile operation and low temperature process.

In this work, a facile, green one-step synthesis technique was applied to fabricate ZnO/CNC hybrids at mild temperature of 80 °C using solely water solvent and bamboo cellulose nanocrystals were used as the biotemplate. The resulting products exhibited nearly spherical, thin sheet and flower-like morphologies at different pH values, and their possible formation mechanism was provided. The effects of different ZnO/CNC hybrids morphologies on the microstructure, antimicrobial, and dye absorption properties were evaluated. Moreover, the antibacterial properties against *Escherichia coli* (*E. coli*, Gram-negative) and *Staphylococcus aureus* (*S. aureus*, Gram-positive) bacteria were tested. We here report a detailed study of absorption properties for methylene blue (MB) and malachite green (MG) on nearly spherical ZnO/CNC hybrids.

2. Experiment

2.1 Materials

Hydrochloric acid (HCl), citric acid (C₆H₈O₇), sodium hydroxide (NaOH), zinc chloride (ZnCl₂), zinc nitrate hexahydrate (Zn(NO₃)₂·6H₂O) and MB (C₁₆H₁₈ClN₃S·3H₂O) were purchased from Guoyao Group Chemical Reagent Co. Ltd (Shanghai, China). MG (C₅₂H₅₄N₄O₁₂) was purchased Shanghai Macklin Biochemical Co. Ltd (Shanghai, China). Bamboo powder was supplied by Zhejiang Provincial Key Laboratory of Chemical Utilization of Forestry Biomass.

2.2 Isolation of CNC

The natural bamboo powder was placed in a plant pulverizer and the 20 mesh sieve components were collected for the preparation of CNC. At room temperature, the bamboo powder was soaked in a 1 mol/L NaOH solution for 12 h, then heated for 2 h at 80 °C with magnetic stirring, and finally washed with distilled water until the pH value kept at about 7 to obtain a higher purity α -Cellulose. The resulting α -Cellulose (8 g) were added into 400 mL HCl (6 mol/L)/citric acid (3 mol/L) mixed aqueous solution (v/v% 9:1). The mixture was heated at 80 °C for 6 h under continuous mechanical stirring. Upon completion, the obtained suspension was neutralized with NaOH aqueous solution until the pH value of the suspension was about 7. The CNC suspension was accumulated by centrifugation (12,000 rpm, 6 min) for three times. Freeze-drying of the CNC suspension at -40 °C for 48 h resulted in powdery CNC and then the rod-like CNC was obtained.

2.3 Preparation of ZnO/CNC hybrids

CNC (1 g) was added into Zn (NO₃)₂·6H₂O solution (0.1 mol/L, 16.8 ml), the pH value of mixture was adjusted to 7 by using NaOH solution (0.5 mol/L). Then, the

mixture was heated to 80 °C. The NaOH solution (0.1 mol/L) was added dropwise to adjust the pH value to 8.5 under mechanical stirring for 30 min. Subsequently, we washed the suspension by centrifugations with deionized water (12,000 rpm at 10 °C for 20 min) after cooling to room temperature. The resulting material was termed ZnO/CNC8.5 sample.

In a typical procedure, 0.4 g of CNC and 0.2726 g of ZnCl₂ were dissolved in 40 mL of distilled water under constant stirring. Then, the pH value of mixture was adjusted to 10.5 and 11.0 by using NaOH solution (0.5 mol/L) respectively. Finally, the mentioned solutions were transferred into two 50 mL of Teflon-lined stainless-steel autoclaves, and hydrothermal growth was carried out at 80 °C for 24 h. After treatment, the resultant autoclaves were rapidly cooled to room temperature. The resulting products are denoted as ZnO/CNC10.5 and ZnO/CNC11.0, respectively. The preparation process and mechanism are shown in Fig. 1.

2.4 Zeta potential test.

The zeta potential values of CNC and ZnO/CNC hybrids in water were measured using a zeta potentiometer (Zetasizer Nano series nano-ZS90, Malvern, UK). A 2.5 mg/mL aqueous suspension of sample was prepared and then diluted to a 0.01% aqueous suspension and measured in triplicate at 25 °C. The average zeta potential values of CNC and ZnO/CNC hybrids were shown in Table 2.

2.5 Carboxyl content analysis.

The carboxyl contents of CNC and ZnO/CNC hybrids were determined by conductivity titration. The dried sample (0.02 g) was added to 0.01 M HCl (50 mL) for

24 hours. Then, 0.1 M NaOH was added dropwise to the mixture so that the pH value was in the range of 2.5 to 3.0. Afterward, 0.01 M NaOH was added at a rate of 0.1 mL/min by using pH stat until pH=7. Finally, the carboxyl contents of the samples were determined from the conductivity and pH curves (Table 2).

2.6 Antibacterial activity determination.

The antibacterial property of the samples was assessed by using *Escherichia coli* (*E. coli*, ATCC 25922) and *Staphylococcus aureus* (*S. aureus*, ATCC 27217) as model Gram-negative and Gram-positive bacteria with qualitative agar disc diffusion method and quantitative mean colony-forming unit method [18]. The antibacterial ratio was determined by counting the microorganism colonies or mean colony-forming units (cfu's) according to the following equation:

$$\text{Antibacterial ratio (\%)} = \left(\frac{N_0 - N}{N_0} \right) \times 100 \quad \text{Eq. (1)}$$

First, two precultures of bacterial cells (*E. coli* and *S. aureus*) were mixed with the fluid medium (concentration 1×10^{-4}), respectively. Then the mixed liquid (100 μ L) was transferred to the solid medium in a sterile environment, and the solution was spread by a disinfected glass rod to cover the surface evenly. The samples (CNC, ZnO/CNC hybrids) were fixed on the culture dishes coated with *E. coli* or *S. aureus* and the dishes were put into the incubator to culture for 24 h at 37 °C. Finally, the inhibition zone was measured. In the mean colony-forming unit method, fresh precultures with fluid medium (100 μ L) of *S. aureus* and *E. coli* were mixed with samples (50 mg) and then set in the incubator (37 °C) for 12 h. Subsequently, the fluid mediums with bacterial cells (1 μ L) were spread on the plates. Viable microorganism colonies can be observed after

incubation of 15 h at 37 °C.

2.7 Absorption experiments

We choose MB and MG as model cationic dyes for wastewater treatment. The absorption experiments were carried out in a batch process with different initial concentrations of dyes. The known weight (50mg) of adsorbent material was added to 50 mL of the dye solutions with an initial concentration of 20 mg/L to 50 mg/L. The contents were shaken thoroughly using a mechanical shaker rotating with a speed of 120 rpm. A certain amount of solution (3 mL) was taken out at preset time intervals and centrifuged to measure the absorbance of the MB dye in the solution using a UV–vis spectrophotometer.

2.7.1 Absorption studies

The removal (R) percentages of MB/MG were calculated using Eq. (2), where q_e and q_t (mg g^{-1}) are the amounts of dye absorbed at equilibrium and time t (min), respectively, following Eq. (3) and Eq. (4).

$$R = \frac{(C_0 - C_t)}{C_0} \times 100 \quad \text{Eq. (2)}$$

$$q_e = \frac{(C_0 - C_e) \times V}{m} \quad \text{Eq. (3)}$$

$$q_t = \frac{(C_0 - C_t) \times V}{m} \quad \text{Eq. (4)}$$

Where C_0 , C_e and C_t represent the initial, equilibrium concentration of dye solutions (mg L^{-1}) and the concentration of dye solution at different time 't', whereas V and m represent the volume of the solution (L) and the mass of the used adsorbent (g), respectively.

2.7.2 Absorption Kinetics models

Lagergren's pseudo-first-order equation, Ho's pseudo-second-order equation, and the intraparticle diffusion model were analyzed to study the time dependence of absorption process and further investigate the absorption mechanisms. The equations used were as follow:

Pseudo-first-order equation:

$$\ln(q_e - q_t) = \ln q_e - k_1 t \quad \text{Eq. (5)}$$

Pseudo-second-order equation:

$$\frac{t}{q_t} = \frac{1}{k_2 \times q_e^2} + \frac{t}{q_e} \quad \text{Eq. (6)}$$

Where q_e and q_t (mg g^{-1}) are the amount of dye absorbed at equilibrium and time t (min), k_1 (min^{-1}) is the pseudo-first-order rate constant, k_2 ($\text{g mg}^{-1} \text{min}^{-1}$) is the pseudo-second-order rate constant.

2.8 Characterization of CNC and ZnO/CNC hybrids

The morphologies of CNC and ZnO/CNC hybrids were characterized by field-emission scanning electron microscopy (FE-SEM, JSM-5610; JEOL, Japan), with the accelerating voltage parameter as 15 kV at room temperature. The potassium bromide (KBr) disc method was used to measure chemical structure via a Fourier-transform infrared (FT-IR) spectrometer (Nicolet 5700, Thermo Electron Corp) at ambient temperature. The wavenumber of FT-IR was scanned at the range 4000-400 cm^{-1} . The optical properties were characterized using UV-vis spectrophotometer (UV, Hitachi U-4150/3900, Japan). The X-ray powder diffraction (XRD) analysis was performed for investigation of crystal phase of the samples. The parameters of the X-ray

powder diffractometer (ARL X'RA, Thermo Electron Corp.) are monochromatic Cu K α radiation at $\lambda = 1.54056 \text{ \AA}$ in the 2θ range $15\text{-}80^\circ$ at a scan rate of 2 deg/min . The X-ray generator tension and current were 40 kV and 30 mA , respectively. The thermostability was observed on thermogravimetric analysis (TGA) analyzer (Pyris Diamond I, PerkinElmer Corp). The samples (about $3\text{-}8 \text{ mg}$) were heated from 30 to $600 \text{ }^\circ\text{C}$ at the rate of 20 K/min under dynamic nitrogen atmosphere with a flow rate of 30 mL/min .

3. Results and discussion

3.1 Morphologies and dimensions.

The morphologies of the CNC and the ZnO/CNC hybrids were characterized by using TEM and FE-SEM, respectively (Fig. 2). The shape of neat CNC was nanorod with the diameter of 10.9 nm and a length of 101.7 nm in Fig. 2a. The pH of the solution was adjusted with NaOH. The anion OH^- was bonded to the cationic Zn^{2+} to form the monomer zinc hydroxide $\text{Zn}(\text{OH})_2$ and $\text{Zn}(\text{OH})_2$ dehydrated to form zinc oxide (ZnO) elementary particles. The shape of the ZnO/CNC hybrids showed different morphologies for each sample depending on the solution pH in Fig. 3. As shown in Fig. 2b, the nearly spherical ZnO nanoparticles with average diameter of 60 nm were obtained at pH 8.5. When pH value was at 8.5, the OH^- concentration was low, while the concentration of the carboxylate anion (COO^-) from carboxyl groups on the CNC template was high. The COO^- competed with OH^- and repelled each other and thus the COO^- anion of CNC was more dominant to attract the cationic Zn^{2+} than the OH^- anion. As the OH^- concentration increased (pH=10.5), the new bonds between $\text{Zn}(\text{OH})_2$

monomers from two adjacent CNC templates were formed and then dehydrated to generate ZnO crystals. The ZnO crystals grew continuously, and eventually formed a two-dimensional sheet-like structure with the diameter 150-500 nm, the length 120-790 nm and the average thickness of 20 nm in Fig. 2c. Moreover, the surface of the sheet was not smooth and crossing sheets were assembled into a three-dimensional network structure. When the OH⁻ concentration continued to increase (pH=11.0), a large amount of OH⁻ and Zn²⁺ to form Zn(OH)₂ monomers. The new bonds are produced after two Zn(OH)₂ monomer dehydration to assemble into ZnO nanoparticles along a certain orientation direction, so many ZnO nanorods with the diameter 120 -330 nm and the length 840-2340 nm were easily assembled into flower-like structure based on CNC template (Fig. 2d). The pH of reaction was shown to have a significant effect on the size and structure of the ZnO nanoparticles. Sheet-like cellulose nanocrystal-zinc oxide nanohybrids were prepared by hydrothermal method in our previous work [19]. Hexagonal sheet-like CNC-ZnO nanohybrid exhibited a smooth surface and the size of ZnO was smaller compared with this work. Different morphologies were modulated by different sources of cellulose template. Mechanisms for modulated morphology/size were different in two works. ZnO microstructures were modified with increasing the molar ratio to CNC by Abdalkarim [8], but the effect on pH values was the dominant mechanism modulating ZnO nanoparticles morphologies in this work. The morphology and size of ZnO/CNC nanohybrid could significantly influence in various properties. The COO⁻ on the surface of CNC template exhibited adsorption on ZnO due to electrostatic attraction. ZnO nanoparticles formed via *in situ* growth. More and more

fine ZnO nanoparticles aggregated on CNC template as pH values increased. It was obvious that zeta potentials shifted from -9.9mV to -8.5mV (Table 2).

3.2 Chemical structures.

To understand the chemical structure of ZnO/CNC hybrids, all the samples were analyzed using FTIR spectroscopy (Fig. 4a). Similar characteristic bands were observed for CNC and ZnO/CNC hybrids, such as peaks at 3,422, 1,603 and 1,048 cm^{-1} related to stretching, bending vibrations of O-H groups [20, 21], and C–O–C stretching of glucose ring skeletal vibration, respectively [22]. Moreover, compared with CNC, a new absorption peak at 600–400 cm^{-1} assigned to Zn–O stretching vibration was found for the ZnO/CNC hybrids [9, 23], illustrating the successful synthesis of ZnO on the CNC template. Zn–O peak locations of ZnO/CNC8.5, ZnO/CNC10.5 and ZnO/CNC11.0 were 463, 433 and 425 cm^{-1} , respectively. It hints a blue shift in the Zn–O absorption peak was observed for ZnO/CNC hybrids with increasing pH values, due to changes in size and morphologies of ZnO nanoparticles. Further, compared to CNC, the in-plane –OH deformation peak position was shifted from 1,637 cm^{-1} to 1603 cm^{-1} for ZnO/CNC8.5, confirming the interaction between CNC and Zn^{2+} [24]. Also, the band intensity of C=O stretching vibration (1,734 cm^{-1}) was decreased for all the hybrids, which was ascribed to strong interactions between oxygen atoms of CNC carboxyl groups and ZnO nanoparticles. The UV–vis results show that strong absorption edge before 400 nm and their absorption of ultraviolet light in the ultraviolet region were found for all the ZnO/CNC hybrids except CNC (Fig. 4b), which further confirmed the successful deposition of ZnO nanoparticles onto the CNC in accord with FTIR results.

3.3 Crystalline structure.

The XRD patterns were further used to estimate crystalline structure of the ZnO/CNC hybrids. The diffraction patterns of the CNCs exhibited typical cellulose I peaks at $2\theta=16.1^\circ$ and 22.4° attributed to (110) and (200) planes [25]. Apart from the characteristic peaks of cellulose, new peaks at 31.9° , 34.5° , 36.3° , 47.7° , 56.8° , 62.9° , 67.9° and 69.3° were found for the ZnO/CNC samples, assigned to (100), (002), (101), (102), (110), (103), (112) and (201) planes of the hexagonal wurtzite-type ZnO [26] in Fig. 4c. This suggests that CNC/ZnO hybrids were successfully fabricated by using CNC as templates. Table 3 records the effect of pH values on crystalline size and crystallinities (χ_c) of ZnO/CNC hybrid samples. In addition, ZnO/CNC8.5 with nearly spherical shape exhibited similar crystalline sizes of 17.5-18.3 nm at three planes, while other two hybrids showed different crystalline sizes, due to different ZnO morphologies (sheet-like and flower cluster shapes). The results were consistent with SEM morphological changes from nearly spherical shape to flower cluster (Fig. 2b-d). Moreover, the χ_c values of the ZnO/CNC hybrids were higher than that of CNC (61.0%). The χ_c values of the hybrids were increased from 63.4% (ZnO/CNC8.5) to 90.1% (ZnO/CNC11.0), indicating more contents of ZnO nanoparticles in the hybrids (Table 2).

3.4 Thermal stability.

The TGA and its derivatives (DTG) curves for CNC and ZnO/CNC hybrids are shown in Fig. 5, and the temperature at 5% weight loss ($T_{5\%}$) is listed in Table 2. Single thermal degradation peaks with one maximum degradation temperature were found for

CNC and the ZnO/CNC hybrids, and indeed thermal degradation of cellulose included depolymerization, dehydration, and decomposition of glycosyl units at degradation temperature of 200-400 °C [27, 28]. $T_{5\%}$ value of CNC was about 288.2 °C, whereas ZnO/CNC hybrids showed higher $T_{5\%}$ values of 312.8- 312.1°C, indicating that the thermal stability of the hybrids was better than CNC. Further, both ZnO/CNC11.0 and ZnO/CNC10.5 gave the better thermal stability than ZnO/CNC8.5, which can be due to more ZnO contents (84.1% and 67.4%) with strong heat shielding effects. In the hybrids, the building blocks (ZnO/CNC8.5) were formed by average 60 nm and near spherical ZnO nanoparticles anchored on the CNC. This contiguous and ordered structural feature, and the strong interaction between the ZnO and CNC subunits made heat transport much easier, consequently, resulting in the ZnO/CNC hybrids being decomposed at a lower temperature [6]. Additionally, limiting oxygen index (LOI) values of CNC and ZnO/CNC hybrids were calculated from char yield (CY) based on equation [13, 29, 47, 49] (Table 2) at 600 °C. The LOI values increased as the char yield increased. The LOI values of all the hybrids were higher than that of CNC, and they were increased from 37.3 for ZnO/CNC8.5 to 51.1 for ZnO/CNC11.0 with increasing pH values. From above, all the hybrids presented the higher LOI values more than 21, demonstrating the great potentials in the fields of excellent flame-resistant materials. High-performance thermally insulating materials using renewable cellulose showed excellent combustion resistance and performed better than traditional fossil fuel insulation. Therefore, the flame-retardant materials with excellent properties based on cellulose had great potential in the field of building insulation applications [50].

3.5 Antimicrobial properties.

The antibacterial activity of the ZnO/CNC hybrids was evaluated against *E. coli* and *S. aureus* with the CNC as control sample. The results of qualitative disc diffusion method are shown in Fig. 6a and b. Fig 6a displayed the antibacterial activities of CNC and ZnO/CNC hybrids against *E. coli*. It is observed that CNC had little antibacterial activity without an inhibition zone. By contrast, ZnO/CNC8.5, ZnO/CNC10.5 and ZnO/CNC11.0 could inhibit the bacterial growth with the inhibition zone of 8.0, 9.0 and 10.0 mm, respectively. The results indicated the effective antibacterial activity of ZnO/CNC hybrids against *E. coli*. This phenomenon clearly indicates that the antibacterial activity was only due to the presence of ZnO, rather than the individual CNC. Fig. 6b shows the antibacterial activities of the samples against *S. aureus*. Compared to CNC without any inhibition zone, ZnO/CNC8.5, ZnO/CNC10.5 and ZnO/CNC11.0 gave obvious inhibition zone of 6.0, 6.3 and 6.7mm, respectively. Furthermore, our results suggest that with the increase of pH values, the inhibition zone of the ZnO/CNC hybrids gradually increased for both bacteria. The antibacterial ratios (99.6%, 99.7%, 99.8%) of three ZnO/CNC hybrids for *E. coli* were higher than the corresponding values (91.4%, 91.6%, 92.1%) for *S. aureus* (Table 2). The antibacterial ratio was calculated by using the quantitative mean colony-forming unit method. Our results suggest that the antibacterial ratio demonstrated a better antibacterial activity of ZnO/CNC hybrids in killing Gram-negative *E. coli*. Combined with the above results, the strong antibacterial activity of ZnO/CNC11.0 was demonstrated for both *E. coli* and *S. aureus* due to incorporating excellent antibacterial ZnO nanoflower clusters and more

ZnO concentrations in the hybrids (Table 2). Some researchers consider that it might be responsible by the formation of hydrogen peroxide (H_2O_2) On ZnO surface [30].

3.6 Absorption capacity of MB and MG

Dyes are widely used to color their products in some industries, such as textiles, dyestuff, paper, and leather. Methylene blue (MB) dye is harmful to fish and other aquatic organisms, which may be liable to permanent injury to human and most aquatic life [31]. Malachite green (MG) is very dangerous, because it is a typical triphenylmethane dye and has highly cytotoxic property against mammalian cells [32]. The present work aims to study a convenient and economic method for MB and MG removal from wastewater by absorption with low cost and abundantly available adsorbents. Therefore, ZnO/CNC hybrid as adsorbents was utilized to investigate the dye removal rate for MB and MG Fig. 7a shows a comparison of dye removal rate of CNC and ZnO/CNC hybrids. The dye removal rate of ZnO/CNC10.5 (85.8%) and ZnO/CNC11.0 (84.3%) was lower than that of CNC, while ZnO/CNC8.5 with the best absorption property gave 93.55% dye removal higher than 91.08% for CNC. At the same time, the dye removal ability of the hybrids decreased with the increase of ZnO content from 37.1% to 71.7 (Table 2), suggesting more ZnO contents on CNC to slightly weaken their dye absorption ability. Generally, the higher dye absorption efficiency of ZnO/CNC hybrids relied on the surface carboxyl group contents, ZnO nanoparticle size and morphology, electrostatic attraction between adsorbent and the dyes (MB/MG) [33, 34]. Indeed, the more carboxyl groups can provide more active absorption sites to remove the dyes [35]. Compared to other hybrids, ZnO/CNC8.5 with more residual

carboxyl groups have more unsaturated binding sites to absorb the most active dyes, resulting in high dye removal rate. Similarly, the CNC with more carboxyl groups also have better dye removal ability. The zeta potential of samples was an important influencing factor on the adsorption capacity. Both MB and MG were positively charged cationic dyes. According to the zeta potentials of hybrids and CNC, the surface charge was negative, which might imply that there was a strong electrostatic interaction between adsorbents and cationic dyes [47, 48]. In this work, CNC from bamboo not only was used to manipulate the morphologies and dispersion of ZnO nanoparticles but also increased absorption property of cationic dyes. During the experiments, we also had observed the degradation capacities of samples to MB dye with continuous stirring under the ultraviolet light for 4 hours. The samples adsorbed the dye quickly, and then the color of the sample hardly changed compared with that in the normal environment (Fig. 7b). The degradation of hybrids to dye was very slow compared with absorption. Therefore, we focus on the investigation of adsorption property of the samples in this work. According to the obtained results, ZnO/CNC8.5 was used as a representative adsorbent to study its absorption performance and absorption mechanism for MB and MG in the subsequent experiments.

3.6.1 Effect of reaction time and initial dye concentration

Fig. 8 a-b shows MB and MG removal efficiency for ZnO/CNC8.5 versus reaction time using various dye concentrations (20, 30, 40, 50 mg/L). The absorption was rapid and the efficiency of removed MB and MG were increased sharply in the first 2 min. The dye removal efficiency of MB and MG reached 97.04% and 98.44% within 5 min

at concentration of 20 mg/L. It is particularly worthy to note that it was very rare to exhibit such rapid and excellent absorption performance in such a short period of time. The increasing trend did not stop until a state of equilibrium was acquired at time of 15 min and the removal efficiency reached 98.36% (20mg/L), 97.61% (30mg/L), 97.39% (40mg/L), 93.55% (50mg/L) of MB and 99.04% (20mg/L), 99.00% (30mg/L), 99.07% (40mg/L), 99.02% (50mg/L) of MG after 60 min, respectively. The rapid absorption at the initial contact time could be attributed to more active absorption sites of the negatively charged groups (carboxyl ions, COO^-) of ZnO/CNC8.5, which can cause attractive forces (electrostatic attractions, van der Waals forces and hydrogen bonding) [36, 37] with positive charge functional groups (quaternary ammonium ion, NR_4^+) of MB molecule. In addition, at lower concentration, the number of the positive charge groups of MB molecules was below the negative charged groups of adsorbents. Subsequently, the fractional absorption became independent with increasing initial concentration. More or less, similar absorption observation for MB and MG was found, while the ZnO/CNC8.5 adsorbent exhibited better removal efficiency on MG dyes absorption. Besides, the removal efficiency of MG increased by 6.3% compared to MB at the same dye concentration. Thus, the ZnO/CNC8.5 hybrid was efficient absorption materials for anionic dye wastewater under mild conditions.

Fig. 8 c-d shows the effects of different initial concentrations (20 to 50 mg/L) on the absorption capacity of MB and MG onto ZnO/CNC8.5 hybrid with increase of contact time. The initial concentration provided an important driving force to overcome mass transfer resistances of all molecules between the aqueous and solid phases [38]. It is

easily observed that the absorption capacity of MB and MG onto the adsorbent drastically increased initially. At lower dye concentrations, almost all the MB and MG molecules could contact with the active sites on the surface of ZnO/CNC8.5. Nevertheless, the absorption sites would reach saturation at high dye concentrations. The absorption equilibrium of ZnO/CNC8.5 increased with the increase of MB and MG concentration and the absorption capacity at the condition of 50mg/L and room temperature reached up to 46.77 mg/g for MB and 49.51 mg/g for MG. The results demonstrated that the actual amount of adsorbed dye per unit mass of ZnO/CNC8.5 was increased with the MB and MG concentrations. This was attributed to increasing in the surface loading of MB on the active vacancies of the adsorbent, which provided availability of more absorption sites on ZnO/CNC8.5. Then the absorption was constant, because the driving force provided by initial dye concentration was hard to overcome the repulsive forces between the dye molecules on the ZnO/CNC8.5 as the available absorption sites gradually decreased. The above results indicated that the ZnO/CNC8.5 hybrid was an effective adsorbent for cationic dyes.

Furthermore, in comparison with other ZnO adsorbents, the excellent absorption capacity of MB by nZORc/BC was documented as much as 0.01701 mg g⁻¹ [35]. The efficiency of MB removal by ZnO was 9.20% in the first 6 min and the maximal MB sorption (7.67 mg g⁻¹) occurred for ZnO within the contact time of 120 min [39]. The adsorption equilibrium of ZnO/CNC hybrids can reach up to 46.77 mg/g for MB and 49.51 mg/g for MG within 60 min in this work, which was greater than most of the ZnO nanocomposite adsorbents.

3.6.2 Absorption kinetics

In order to understand the absorption process, absorption kinetic study was carried out to understand the absorption mechanism, which was important for efficiency and performance of the absorption process. The experimental data of MB and MG absorption on ZnO/CNC8.5 hybrid was fitted using the pseudo-first-order Eq. (5) and pseudo-second-order kinetic models Eq. (6). The k_1 , k_2 , q_e , and calculated $q_{e,cal}$ values are shown in Table 4, The values of k_1 and $q_{e,cal}$ can be determined from the slope and intercept in the plot of $\ln(q_e - qt)$ vs t Fig. 9a and Fig. 9c. The $q_{e,cal}$ of the pseudo-first-order model deviated from the experimental q_e for all the samples (from 20 to 50 mg/L). Moreover, the correlation coefficients R^2 for the first-order kinetic model were only above 0.62218 for MB and above 0.40037 for MG. The values of k_2 and $q_{e,cal}$ at various concentrations were obtained through the intercept and the slope of the linear plots of (t/q_t) vs t . The linear plots of t/q_t versus t showed a good fit between experimental ($q_{e(exp)}$) and calculated ($q_{e(cal)}$) values from pseudo-second-order model (Fig. 9b and Fig. 9d). The R^2 values for this model were greater than 0.99999 at all the tested concentrations, which were thus higher than the R^2 value obtained from the pseudo-first-order model. For ZnO/CNC8.5 hybrid, the q_e values of MB and MG were 46.6 and 49.7 mg/g, respectively. It suggests that the absorption data were well represented by pseudo-second-order kinetic model, and the absorption capacity values q_e increased with increase of initial concentration of MB and MG dyes at concentrations of 20-50 mg/L.

The FTIR spectra of the ZnO/CNC8.5 before and after the MB and MG absorption

were shown in Fig. 10. The spectra implicated the presence of various functional groups detected in the surface of ZnO/CNC8.5. The surface of ZnO/CNC8.5 has abundant hydroxyl groups and the bands at 3422 cm^{-1} exhibited a slight displacement (3419 cm^{-1}) [40], which revealed that O–H played an important role for MB absorption onto the ZnO/CNC8.5. Furthermore, the absorption peaks at 1593 , 1386 and 1324 cm^{-1} , being assigned to the vibration of aromatic ring, C–N bond, and CH_3 group for MB, respectively [41] and the sharp absorption peak at around 1053 cm^{-1} were due to C–O stretching vibrations. These peaks could be found in the FTIR spectrum of the ZnO/CNC8.5 after the MB absorption. These results revealed the presence of various functional groups in MB detected on the adsorbent surface during the absorption. It should be noted that the peaks seem to be a significant decrease in intensity after MB absorption, which might be resulted from the interactions between ZnO/CNC8.5 and MB. The negatively charged surfaces of the adsorbent could provide absorption sites for electrostatic interaction and hydrogen bonding with cationic MB dye.

Absorption band at 1613 cm^{-1} corresponded to the aromatic ring stretching vibration on MG, which was shifted to 1619 cm^{-1} for ZnO/CNC8.5 after absorption. The C=C stretching of the aromatic ring, aromatic tertiary amine and tertiary amine C–N stretching vibrations [42] were shifted from 1587 , 1372 , 1218 cm^{-1} to 1599 , 1384 and 1236 cm^{-1} , respectively. Furthermore, the intensity decreased after MG absorption. The above drastic differences could well define the appearance or absorption of MG onto ZnO/CNC8.5 surface. The peaks at 1632 and 1111 cm^{-1} corresponding to C=O and C–O of citrate carboxylate groups slightly shifted to 1634 cm^{-1} , 1114 cm^{-1} and their intensity

decreased a lot, which may be attributed to electrostatic attraction between negative charged carboxylate anion of ZnO/CNC8.5 and positive charged MG. Additionally, the band between 3200–3500 cm^{-1} was indicative of stretching vibration of N-H and O-H, the 3241 cm^{-1} peak of N-H was overlapped by 3422 cm^{-1} peak of O-H. Also, the peak at 1034 cm^{-1} corresponding to C-O of alcohols slightly shifted to 1036 cm^{-1} [43]. These changes could be due to hydrogen bonds between -OH of carboxylate groups on ZnO/CNC8.5 and MG. Besides, the properties of nanoscale effect and near spherical morphology could make ZnO/CNC8.5 microspheres contact and absorb MG molecules efficiently. These aspects mentioned above synergistically contributed to the high absorption capacity and removal efficiency of ZnO/CNC8.5 for both MB and MG.

4. Conclusions

Various morphologies of ZnO/CNC hybrids (nearly spherical, thin-sheet and flower-like shapes) were successfully prepared by using bamboo CNC as templates. In addition, the effect of pH values on ZnO morphologies and properties of ZnO/CNC hybrids were studied in detail. It is found that low pH value (8.5) would induce formation of nearly spherical shape hybrids with an average diameter of about 60 nm because of low OH^- concentration. Under high pH values (10.5 and 11.0), sheet-like and flower-like hybrids were obtained due to the large quantity of OH^- . Besides, both sheet-like and flower-like hybrids had high crystallinity and ZnO contents, leading to higher thermal stability for them. However, spherical ZnO/CNC8.5 hybrids showed smaller size and more carboxyl groups (low crystallinity), resulting in higher dye

absorption capacity for MB and MG dyes. Thus, ZnO/CNC8.5 as a representative model sample were chosen to investigate influence of initial concentration and contact time on dye removal rate and absorption kinetic studies. The dye absorption was rapid in the first 2 min and the dye removal rate of MB and MG reached over 91.47% and 97.85% within 5 min. The absorption kinetics accurately described by the pseudo-second-order model with high R^2 . Electrostatic attraction between carboxyl groups(COO^-) and positive charge functional groups (NR_4^+) was the main absorption mechanisms for the dye absorption of hybrids. Therefore, such hybrids with improved properties show great potential for use as excellent adsorbent of cationic dye in industrial wastewater.

Acknowledgments

The work is funded by Key Program for International S &T Innovation Cooperation Projects of China [2016YFE0131400], Integrated project of green manufacturing and recycling system for waste textiles, Ministry of industry and information technology of China, State Key Laboratory for Modification of Chemical Fibers and Polymer Materials, Donghua University [LK1713], Zhejiang Province welfare technology applied research project [LGC19E030002] and Candidates of Young and Middle Aged Academic Leader of Zhejiang Province, “521” Talent Project of Zhejiang Sci-Tech University, and the Young Elite Scientists Sponsorship Program by CAST.

References

- [1] S. Y. H. Abdalkarim, H. Y. Yu, D. Wang, J. Yao, Electrospun poly (3-hydroxybutyrate-co-3-hydroxy-valerate)/cellulose reinforced nanofibrous

- membranes with ZnO nanocrystals for antibacterial wound dressings, *Cellulose*. 24 (2017) 2925-2938.
- [2] F. Fu, J. Gu, X. Xu, Q. Xiong, Y. Zhang, X. Liu, & J. Zhou, Interfacial assembly of ZnO–cellulose nanocomposite films via a solution process: a one-step biomimetic approach and excellent photocatalytic properties, *Cellulose*. 24 (2017) 147-162.
- [3] A. Kumar, H. Gullapalli, K. Balakrishnan, A. Botello - Mendez, R. Vajtai, M. Terrones, P. M. Ajayan, Flexible ZnO–cellulose nanocomposite for multisource energy conversion, *Small*. 7 (2011) 2173-2178.
- [4] E. Lizundia, A. Urruchi, J. L. Vilas, L. M. León, Increased functional properties and thermal stability of flexible cellulose nanocrystal/ZnO films, *Carbohyd. Polym.* 136 (2016) 250-258.
- [5] R. J. Moon, A. Martini, J. Nairn, J. Simonsen, J. Youngblood, Cellulose nanomaterials review: structure, properties and nanocomposites, *Chem. Soc. Rev.* 40 (2011) 3941-3994.
- [6] S. W. Zhao, M. Zheng, X. H. Zou, Y. Guo, Q. J. Pan, Self-assembly of hierarchically structured cellulose@ ZnO composite in solid–liquid homogeneous phase: synthesis, DFT calculations, and enhanced antibacterial activities, *ACS. Sustain. Chem. Eng.* 5 (2017) 6585-6596.
- [7] M. Kaushik, A. Moores, nanocelluloses as versatile supports for metal nanoparticles and their applications in catalysis, *Green Chem.* 18 (2016) 622-637.
- [8] S. Y. H. Abdalkarim, H. Y. Yu, C. Wang, L. Yang, Y. Guan, L. Huang, J. Yao, Sheet-like cellulose nanocrystal-ZnO nanohybrids as multifunctional reinforcing

- agents in biopolyester composite nanofibers with ultrahigh UV-Shielding and antibacterial performances, *ACS. Appl. Bio.Mater.* 1 (2018) 714-727.
- [9] S. Azizi, M. Ahmad, M. Mahdavi, S. Abdolmohammadi, Preparation, characterization, and antimicrobial activities of ZnO nanoparticles/cellulose nanocrystal nanocomposites. *BioResources*, 8 (2013) 1841-1851.
- [10] A. Kołodziejczak-Radzimska, & T. Jesionowski, Zinc oxide—from synthesis to application: a review, *Materials*. 7 (2014) 2833-2881.
- [11] M. M. Tomczak, M. K. Gupta, L. F. Drummy, S. M. Rozenzhak, R. R. Naik, Morphological control and assembly of zinc oxide using a biotemplate, *Acta. Biomater.* 5 (2009) 876-882.
- [12] K. Lefatshe, C. M. Muiva, L. P. Kebaabetswe, Extraction of nanocellulose and in-situ casting of ZnO/cellulose nanocomposite with enhanced photocatalytic and antibacterial activity, *Carbohydr. Polym.* 164 (2017) 301-308.
- [13] R. T. Yang, H. Y. Yu, M. L. Song, Y. W. Zhou, J. M. Yao, Flower-like zinc oxide nanorod clusters grown on spherical cellulose nanocrystals via simple chemical precipitation method, *Cellulose*. 23 (2016) 1871-1884.
- [14] H. Y. Yu, G. Y. Chen, Y. B. Wang, J. M. Yao, A facile one-pot route for preparing cellulose nanocrystal/zinc oxide nanohybrids with high antibacterial and photocatalytic activity, *Cellulose*. 22 (2015) 261-273.
- [15] A. Bendahou, H. Kaddami, A. Dufresne, Investigation on the effect of cellulosic nanoparticles' morphology on the properties of natural rubber based nanocomposites, *Eur. Polym. J.* 46 (2010) 609-620.

- [16] V. Khoshkava, M. R. Kamal, Effect of cellulose nanocrystals (CNC) particle morphology on dispersion and rheological and mechanical properties of polypropylene/CNC nanocomposites, *ACS. Appl. Mater. Inter.* 6 (2014) 8146-8157.
- [17] T. Zimmermann, E. Pöhler, P. Schwaller, Mechanical and morphological properties of cellulose fibril reinforced nanocomposites, *Adv. Eng. Mater.* 7 (2005) 1156-1161.
- [18] Q. Xu, Y. Wu, Y. Zhang, F. Fu, X. Liu, Durable antibacterial cotton modified by silver nanoparticles and chitosan derivative binder. *Fiber. Polym.* 17 (2016) 1782-1789.
- [19] S. Y. H. Abdalkarim, H. Y. Yu, C. Wang, L. X. Huang, J. Yao, Green synthesis of sheet-like cellulose nanocrystal–zinc oxide nanohybrids with multifunctional performance through one-step hydrothermal method, *Cellulose.* 25 (2018) 6433-6446.
- [20] Q. Lu, W. Lin, L. Tang, S. Wang, X. Chen, B. Huang, A mechanochemical approach to manufacturing bamboo cellulose nanocrystals, *J. Mater. Sci.* 50 (2015) 611-619.
- [21] Y. Hu, L. Tang, Q. Lu, S. Wang, X. Chen, B. Huang, Preparation of cellulose nanocrystals and carboxylated cellulose nanocrystals from borer powder of bamboo, *Cellulose.* 21 (2014) 1611-1618.
- [22] H. S. Bhatti, S. Kumar, K. Singh, Structural and optical characterization of hydroxy-propyl methyl cellulose-capped ZnO nanorods, *J. Mater. Sci.* 48 (2013)

5536-5542.

- [23] A. Wei, L. Xiong, L. Sun, Y. Liu, W. Li, W. Lai, X. Liu, L. Wang, W. Huang, X. Dong, One-step electrochemical synthesis of a graphene–ZnO hybrid for improved photocatalytic activity, *Mater. Res Bull.* 48 (2013) 2855-2860.
- [24] S. A. Ovalle-Serrano, V. S. Carrillo, C. Blanco-Tirado, J. P. Hinestroza, M. Y. Combariza, Controlled synthesis of ZnO particles on the surface of natural cellulosic fibers: effect of concentration, heating and sonication, *Cellulose.* 22 (2015) 1841-1852.
- [25] B. S. Brito, F. V. Pereira, J. L. Putaux, B. Jean, Preparation, morphology and structure of cellulose nanocrystals from bamboo fibers, *Cellulose.* 19 (2012) 1527-1536.
- [26] C. Katepetch, R. Rujiravanit, H. Tamura, Formation of nanocrystalline ZnO particles into bacterial cellulose pellicle by ultrasonic-assisted in situ synthesis, *Cellulose.* 20 (2013) 1275-1292.
- [27] M. A. Henrique, W. P. F. Neto, H. A. Silvério, D. F. Martins, L. V. A. Gurgel, H. D. S. Barud, Kinetic study of the thermal decomposition of cellulose nanocrystals with different polymorphs, cellulose i and ii, extracted from different sources and using different types of acids, *Ind. Crop. Prod.* 76 (2015)128-140.
- [28] T. Kosuda, T. Okada, S. Nozaka, Y. Matsuzawa, T. Shimizu, S. Hamanaka, S. Mishima, Characteristics and mechanism of low temperature dehydrochlorination of poly (vinyl chloride) in the presence of zinc (II) oxide, *Polym. Degrad. Stabil.* 97 (2012) 584-591.

- [29] Y. Zhou, H. Y. Yu, J. P. Gu, J. Y. Zhu, M. H. Zhu, Y. Guan, J. M. Yao, Novel fabrication of modulated carpenterworm-like zinc oxide/polyacrylonitrile composite nanofibers for photocatalytic degradation of methylene blue dye, *J. Taiwan. Inst. Chem. E.* 91 (2018) 548-555.
- [30] Y. Jiang, L. Zhang, D. Wen, Y. Ding, Role of physical and chemical interactions in the antibacterial behavior of ZnO nanoparticles against *E. coli*, *Mater. Sci. Eng. C.* 69 (2016) 1361-1366.
- [31] S. Shakoor, A. Nasar, Removal of methylene blue dye from artificially contaminated water using citrus limetta peel waste as a very low cost adsorbent, *J. Taiwan. Inst. Chem. E.* 66 (2016) 154-163.
- [32] S. Srivastava, R. Sinha, D. Roy, Toxicological effects of malachite green, *Aquat. Toxicol.* 66 (3) (2004) 319-329.
- [33] M. Ghaedi, H. Karimi, F. Yousefi, Silver and zinc oxide nanostructures loaded on activated carbon as new adsorbents for removal of methylene green: A comparative study, *Hum. Exp. Toxicol.* 33 (2014) 956-967.
- [34] N. Gupta, A. K. Kushwaha, M. C. Chattopadhyaya, Application of potato (*Solanum tuberosum*) plant wastes for the removal of methylene blue and malachite green dye from aqueous solution, *Arab. J. Chem.* 9 (2016) S707-S716.
- [35] D. C. Wang, H. Y. Yu, X. Fan, J. Gu, S. Ye, J. Yao, Q. Q. Ni, High Aspect Ratio Carboxylated Cellulose Nanofibers Crosslinked to Robust Aerogels for Superabsorption– flocculants: Paving Way from Nano– Scale to Macro– Scale, *ACS. Appl. Mater. Inter.* 10 (2018) 20755–20766.

- [36] M. Doğan, H. Abak, M. Alkan, Adsorption of methylene blue onto hazelnut shell: kinetics, mechanism and activation parameters, *Journal of Hazardous Materials*. 164 (2009) 172-181.
- [37] P. Zhang, D. Hou, D. O'Connor, X. Li, S. O. Pehkonen, R. S. Varma, X. Wang, Green and Size-Specific Synthesis of Stable Fe-Cu Oxides as Earth-Abundant Adsorbents for Malachite Green Removal, *ACS. Sustain. Chem. Eng.* 6 (2018) 9229–9236.
- [38] J. Shu, R. Liu, H. Wu, Z. Liu, X. Sun, C. Tao, Adsorption of methylene blue on modified electrolytic manganese residue: Kinetics, isotherm, thermodynamics and mechanism analysis, *J. Taiwan. Inst. Chem. E.* 82 (2018) 351-359.
- [39] I. K. Al-Khateeb, M. S. Mahmood, Adsorption, Thermodynamics and Kinetics of Methylene Blue on Nano Structured ZnO Crystals, *Am. Chem. Sci. J.* 13 (2016) 1-9.
- [40] J. Fu, Z. Chen, M. Wang, S. Liu, J. Zhang, J. Zhang, Q. Xu, Adsorption of methylene blue by a high-efficiency adsorbent (polydopamine microspheres): kinetics, isotherm, thermodynamics and mechanism analysis, *Chem. Eng. J.* 259 (2015) 53-61.
- [41] J. Tan, Y. Wang, M. Liu, C. He, Adsorption of thorium from aqueous solution by poly (cyclotriphosphazene-co-4, 4'-sulfonyldiphenol), *J. Radioanal. Nucl. Ch.* 314 (3) (2017) 2243-2252.
- [42] H. Tang, W. Zhou, L. Zhang, Adsorption isotherms and kinetics studies of malachite green on chitin hydrogels, *J. Hazard. Mater.* 209 (2012) 218-225.

- [43] L. Len, X. Yuan, G. Zeng, J. Shao, X. Chen, Z. Wu, H. Wang, X. Peng, Surface characterization of rice husk bio-char produced by liquefaction and application for cationic dye (Malachite green) adsorption, *Fuel*. 155 (2015) 77-85.
- [44] H. Xiao, W. Zhang, Y. Wei, L. Chen, Carbon/ZnO nanorods composites templated by TEMPO-oxidized cellulose and photocatalytic activity for dye degradation, *Cellulose*. 25 (2018) 1809-1819.
- [45] M. Yadollahi, I. Gholamali, H. Namazi, M. Aghazadeh, Synthesis and characterization of antibacterial carboxymethyl cellulose/ZnO nanocomposite hydrogels, *Int. J. Bio. Macromol.* 741 (2015) 36-141.
- [46] P. L. Bhutiya, M. S. Mahajan, M. A. Rasheed, M. Pandey, S. Z. Hasan, N. Misra, Zinc oxide nanorod clusters deposited seaweed cellulose sheet for antimicrobial activity, *Int. J. Bio. Macromol.* 112 (2018) 1264-1271.
- [47] H. Y. Yu, D. Z. Zhang, F. F. Lu, J. M. Yao, New approach for single-step extraction of carboxylated cellulose nanocrystals for their use as adsorbents and flocculants, *ACS. Suatain. Chem. Eng.* 4 (2016)2632-2643.
- [48] R. Marsalek, Particle size and zeta potential of ZnO, *APCBEE procedia*, 9 (2014) 13-17.
- [49] M. Trigo-López, Á. Miguel-Ortega, S. Vallejos, A. Muñoz, D. Izquierdo, Á. Colina, F. García, J. M. García, Intrinsically colored wholly aromatic polyamides (aramids), *Dyes. Pigments*. 122 (2015) 177-183.
- [50] B. Wicklein, A. Kocjan, G. Salazar-Alvarez, F. Carosio, G. Camino, M. Antonietti, L. Bergström, Thermally insulating and fire-retardant lightweight anisotropic

foams based on nanocellulose and graphene oxide, Nat. Nanotechnol. 10 (2015)

277.

ACCEPTED MANUSCRIPT

Figure Captions

Fig. 1 Preparation process and formation mechanism of ZnO/CNC hybrids.

Fig. 2 FE-SEM images of CNC and ZnO/CNC hybrids.

Fig. 3 Schematic diagram for the growth of ZnO/CNC nanostructures at different pH.

Fig. 4 (a) FTIR spectra of CNC and ZnO/CNC hybrids, (b) UV-vis absorbance spectra of CNC and ZnO/CNC hybrids, (c) XRD patterns of CNC and ZnO/CNC hybrids.

Fig. 5 TGA (a) and DTG (b) curves of CNC and ZnO/CNC hybrids.

Fig. 6 Antibacterial ability of CNC and ZnO/CNC hybrids against *E. coli*. (a) and *S. aureus* (b).

Fig. 7 Dye removal of CNC and ZnO/CNC hybrids (a), sample color change before and after MB adsorption under the ultraviolet light for 4 hours (b).

Fig. 8 Effect of contact time on the removal efficiency of MB (a) and MG (b) with the ZnO/CNC8.5, the variation of adsorption capacity with adsorption time at various initial concentrations: MB (c) and MG (d).

Fig. 9 Adsorption kinetic models of MB onto the ZnO/CNC8.5 hybrid: (a) pseudo-first order model, (b) pseudo-second-order model; adsorption kinetic models of MG onto the ZnO/CNC8.5 hybrid: (c) pseudo-first order model, (d) pseudo-second-order model.

Fig. 10 FTIR spectra of ZnO/CNC8.5 before and after adsorption of MB (a) and MG (b)

Table 1 Summary on synthesis methods and morphologies of functional ZnO/CNC hybrids using CNCs as templates.

Table 2 Antibacterial activity and other parameters for CNC and ZnO/CNC hybrids prepared under different pH values

Table 3 Average crystallite size and crystallinity for CNC and ZnO/CNC hybrids prepared under different pH values.

Table 4 Constants and correlation coefficients of pseudo-first order and pseudo-second order kinetic models for adsorption of MB and MG onto the ZnO/CNC hybrids.

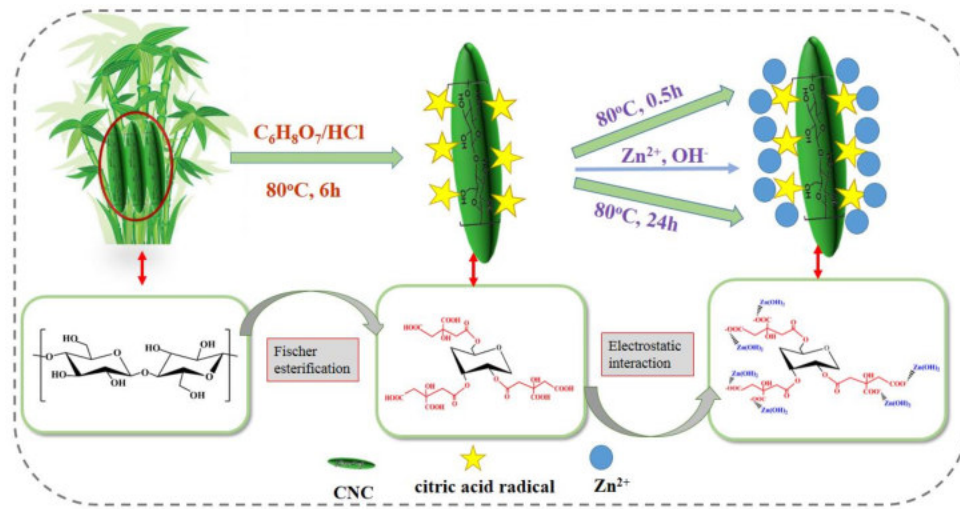
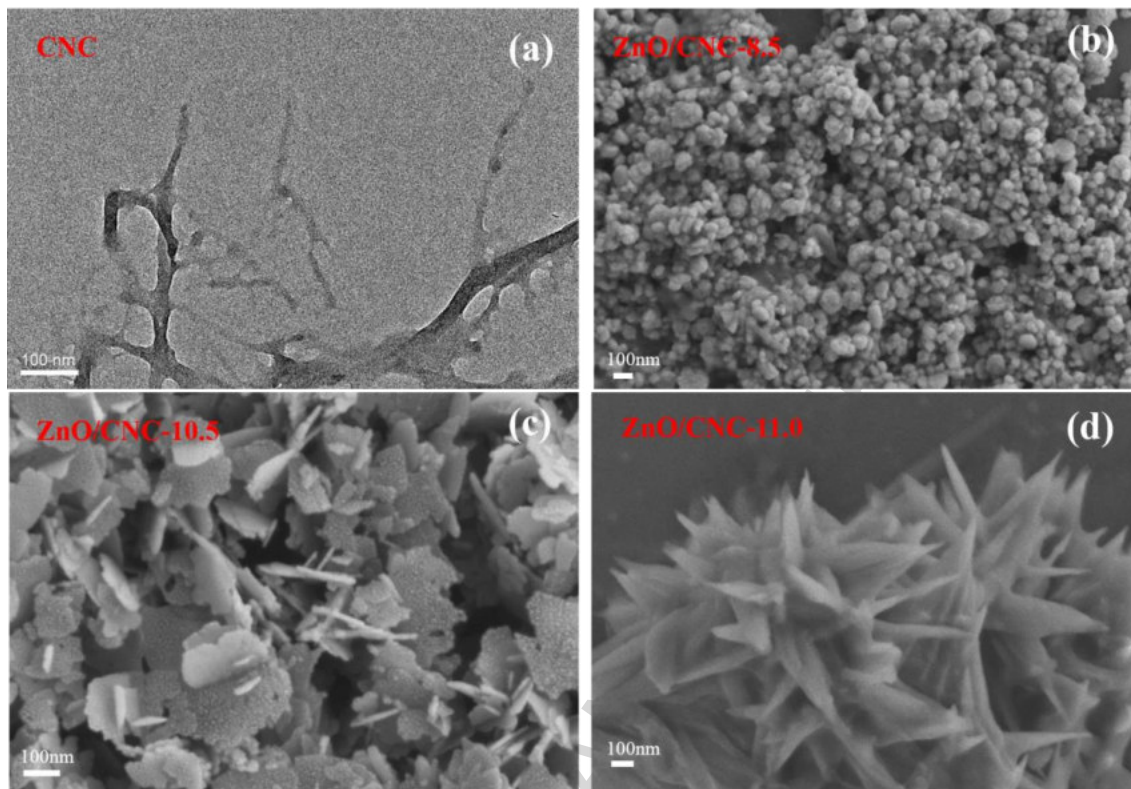


Fig. 1

**Fig. 2**

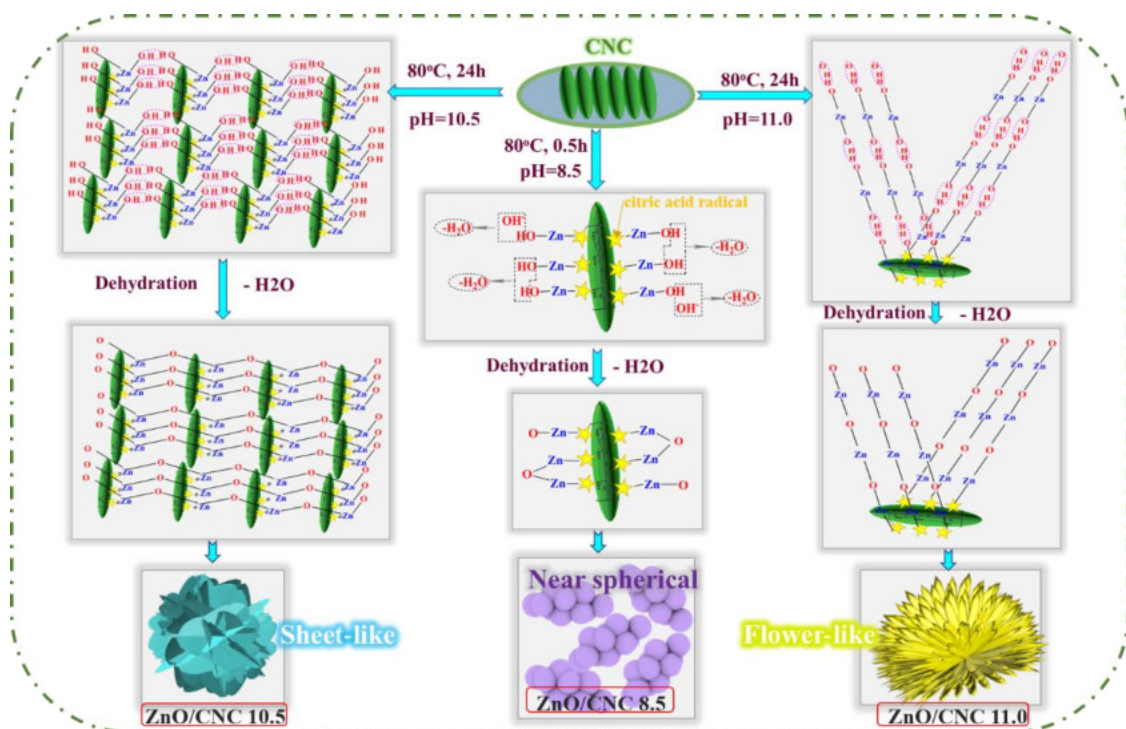


Fig. 3

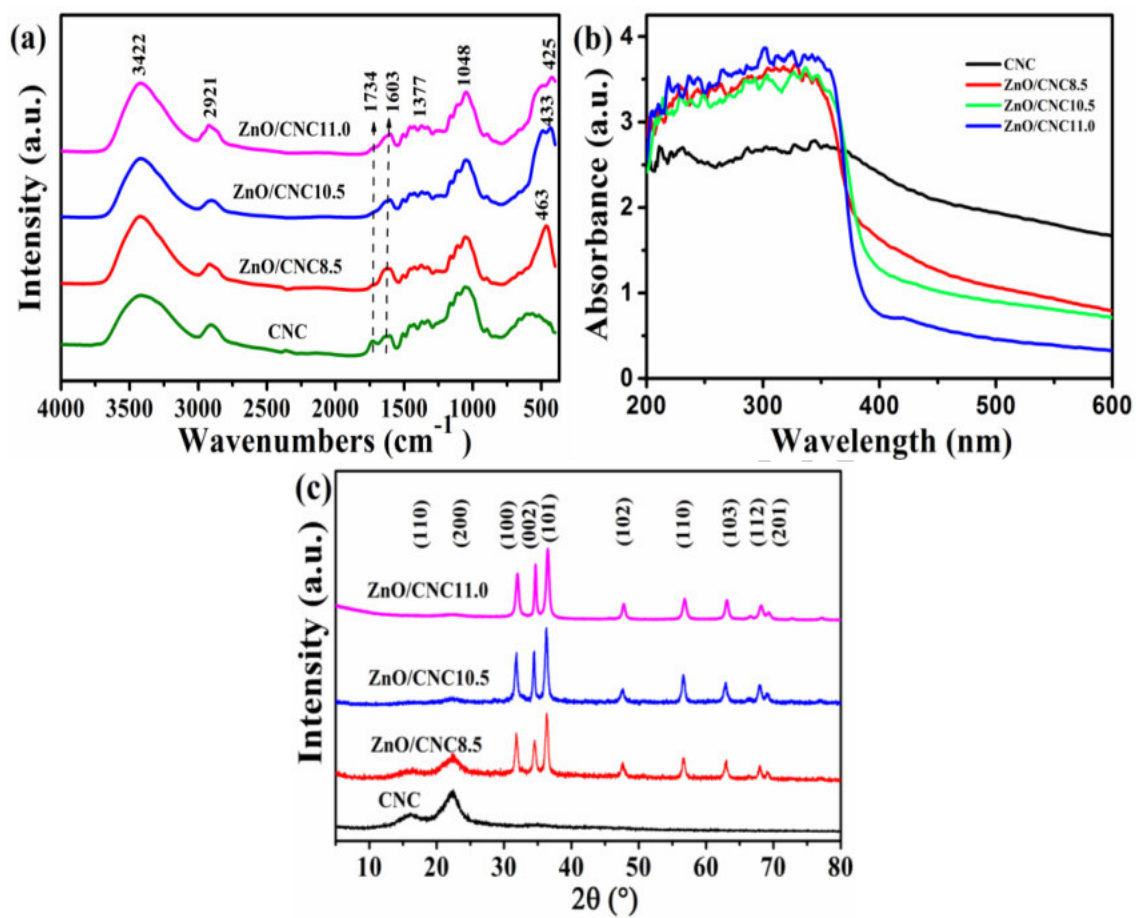


Fig. 4

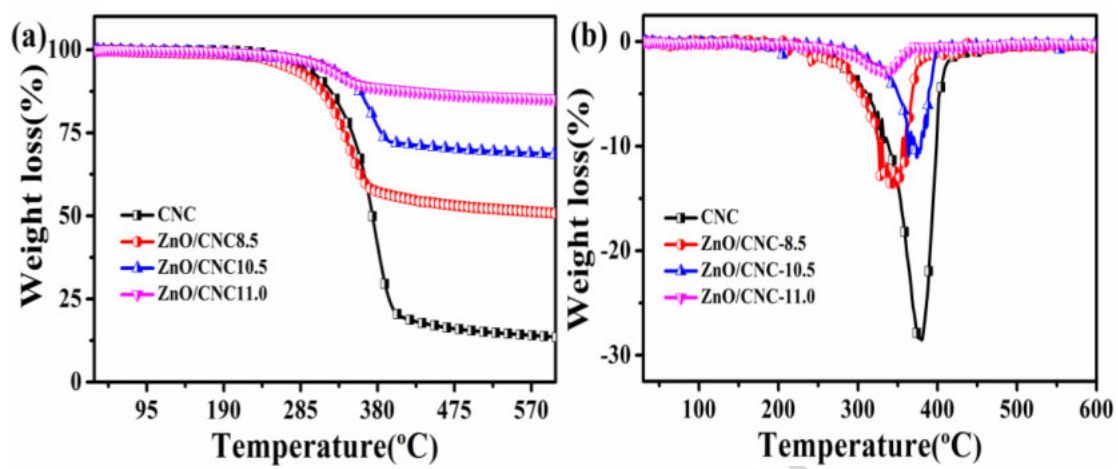


Fig. 5

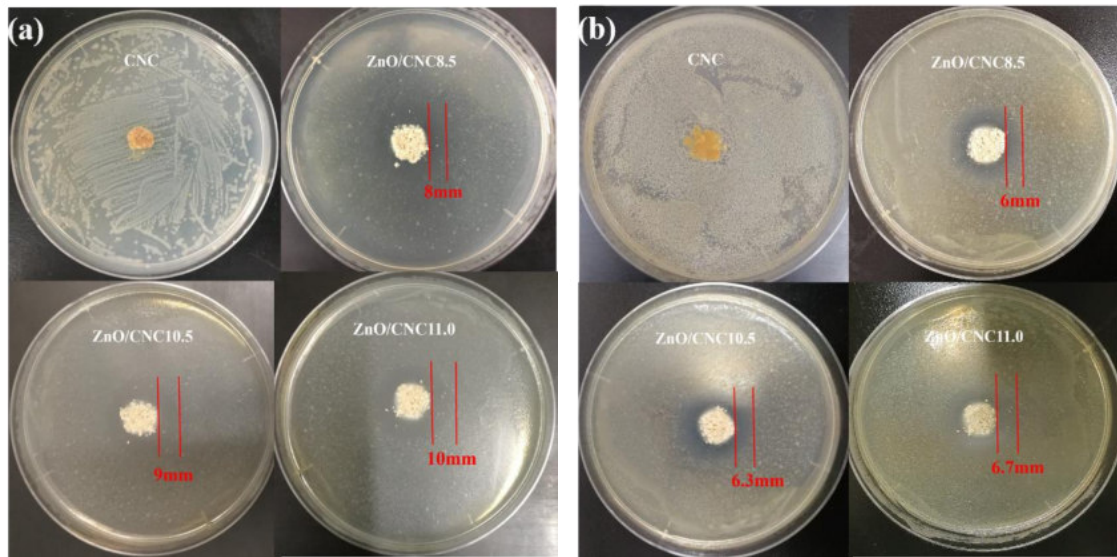


Fig. 6

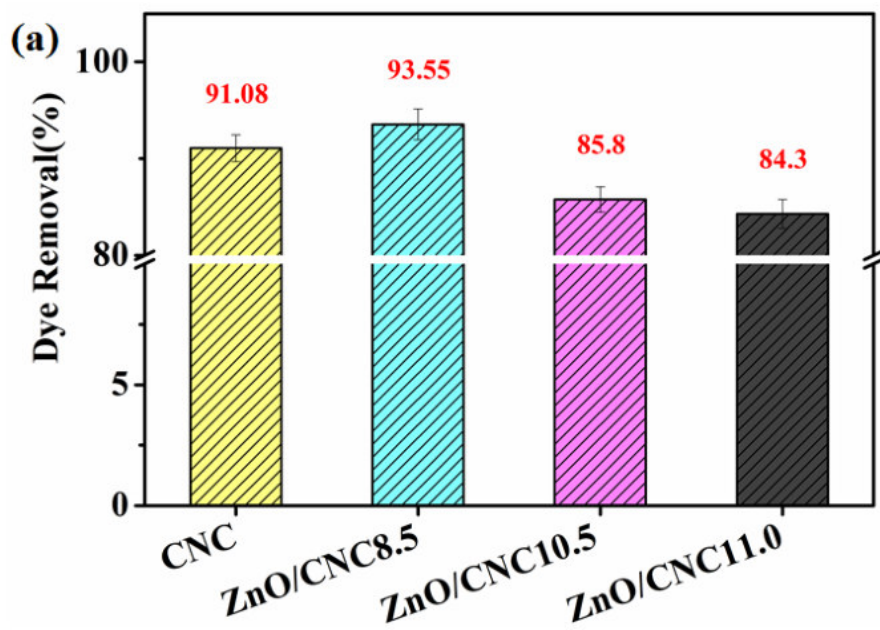


Fig. 7a

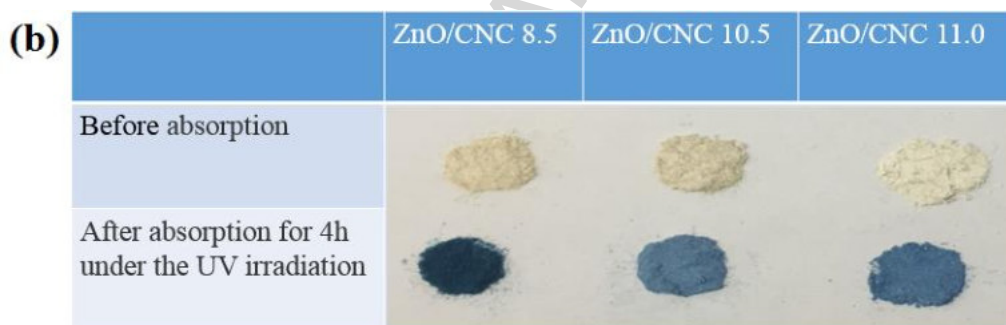


Fig. 7b

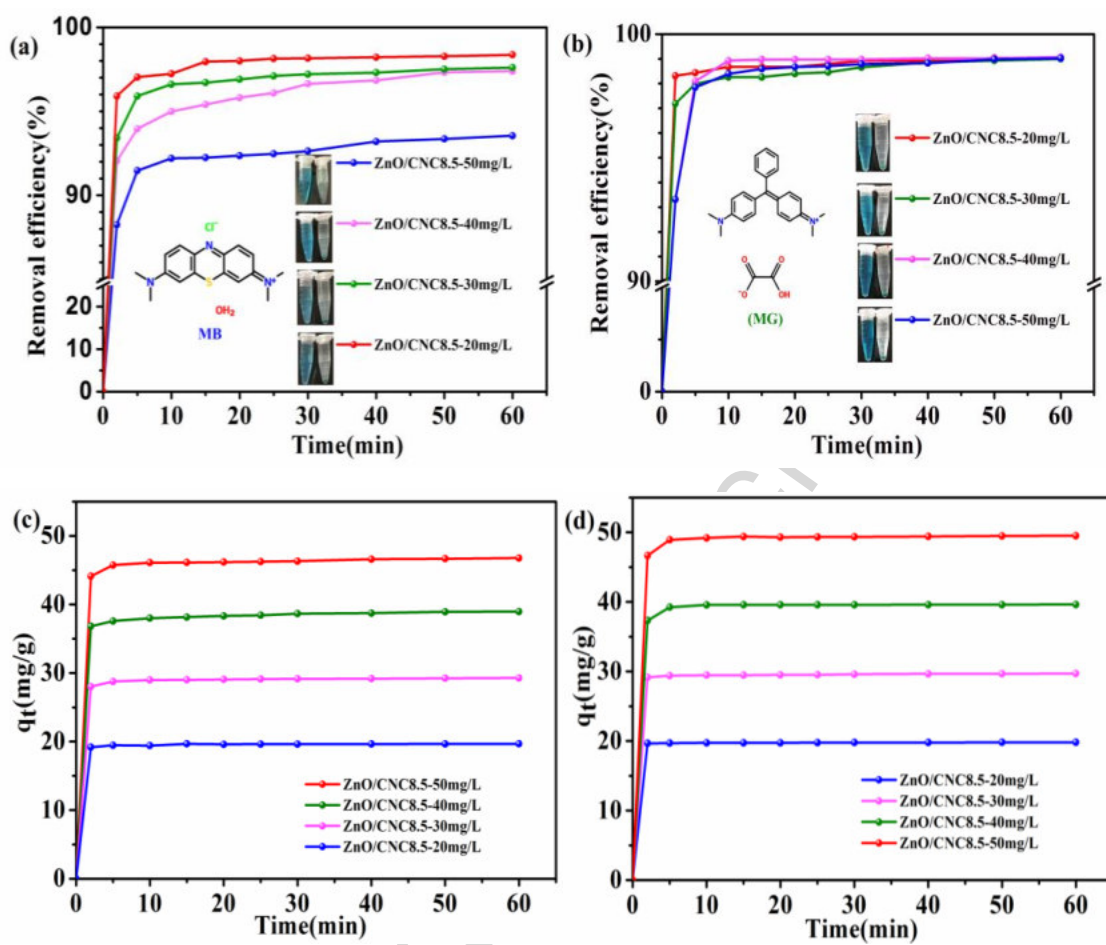


Fig. 8

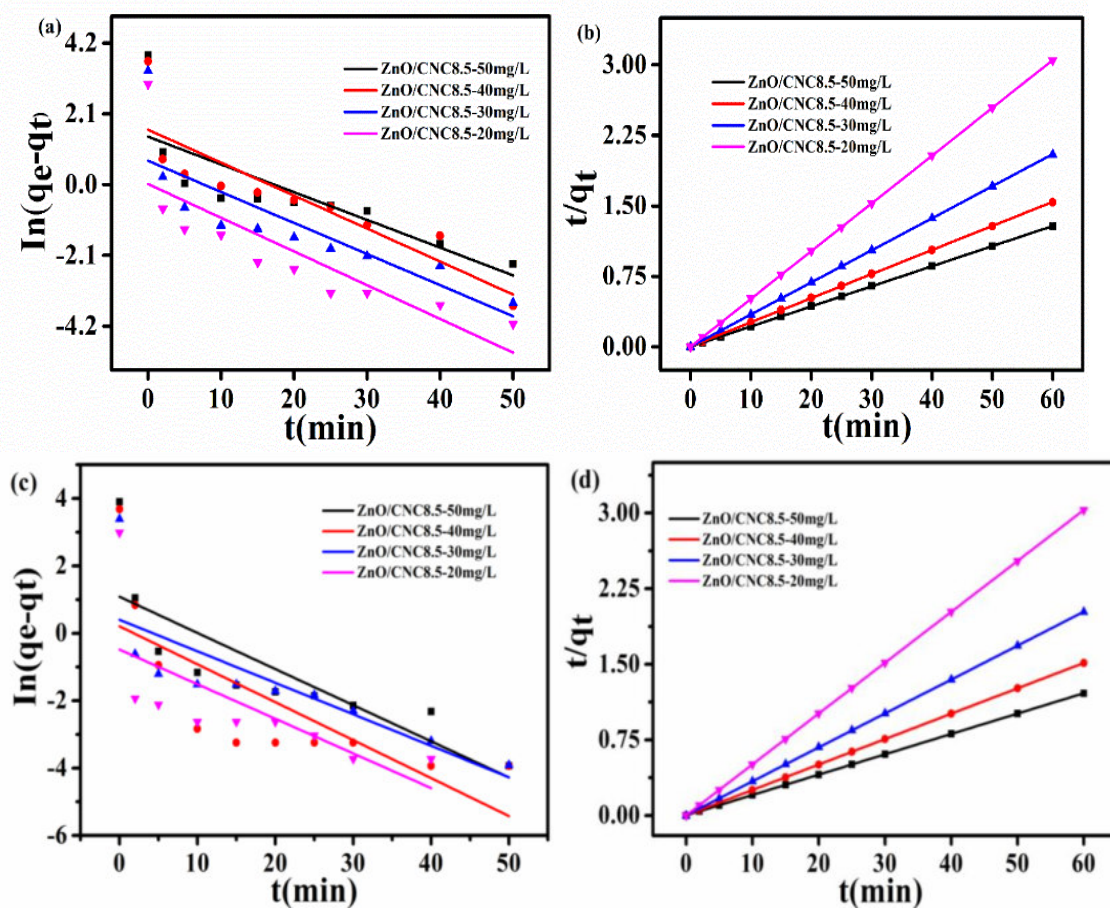


Fig. 9

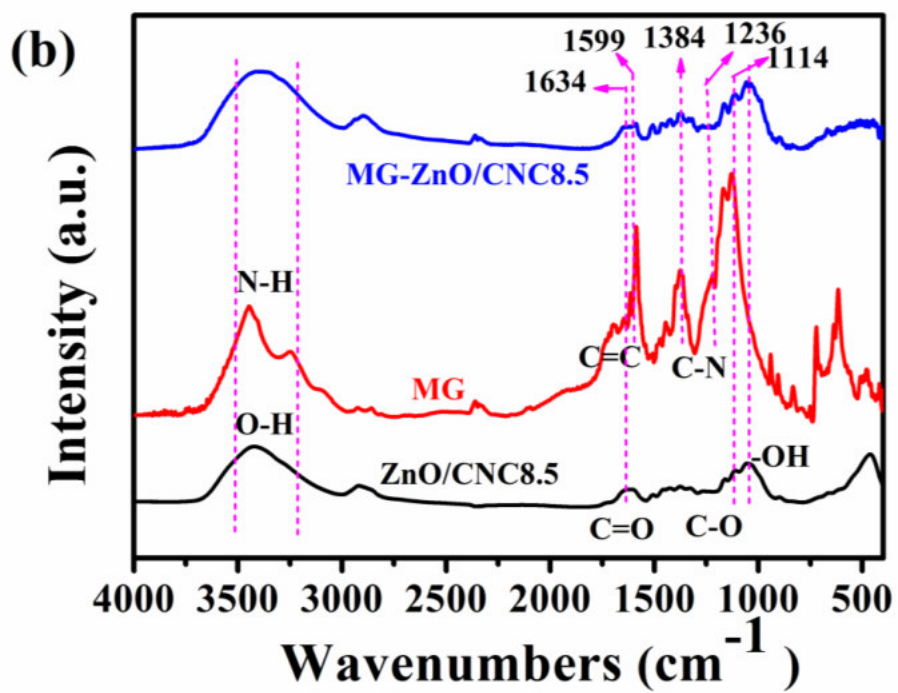


Fig. 10

Table 1 Summary on synthesis methods and morphologies of functional ZnO/CNC hybrids using CNCs as templates.

Method	Nanocellulose source	Morphology	Mechanism	for	Applications/properties	Ref.
Precipitation	Filter paper CNC	Hexagonal shapes	Average ZnO size increased by increasing the weight ratio of Zn(AC) ₂ 2H ₂ O to CNC	shape/size modulated	Antibacterial property	[9]
Low temperature precipitation	Bamboo pulp	Nanosheets and nanorods	Nanosheets and nanorods increase of carboxyl of carboxyl of TEMPO-oxidized cellulose	to with the	Photocatalytic activity	[44]
Reduction and precipitation	CMC	Nanoscaled ZnO	ZnO nanocomposites compared by two preparation routes	Adsorption and degradation		[35]
Bottom-up synthesis	Hydroxypropyl methyl cellulose	Nanorods with wurtzite structure	The aspect ratio of nanorods enhanced by increasing HPMC	ratio of was with	Photocatalytic property	[22]

				concentration		
Hydrotherma l method	cellulose	Nano microscale ZnO particles	and and	Nano and microscale ZnO particles prepared with the increasing of pH	Antibacterial Activity	[6]
Ultrasonic-as sisted in situ synthesis	Bacterial cellulose	Cauliflower fungus-like structure		ZnO crystalline size were determined by the immersion time and ultrasonic treatment time	Antibacterial activity	[26]
In formation	situ CMC	Spherical particles		ZnO nanoparticles size were influenced by zinc nitrate concentration	Antibacterial effects	[45]
Single step hydrothermal method	Seaweed cellulose	Flower-like ZnO nanorod clusters		Length and diameter of ZnO nanorods depend on the concentration of mineralizer	Antibacterial activity	[46]
Hydrotherma l method	MCC	Sheet-like microstructur es		ZnO microstructures were modified by the molar ratio to CNC	UV-shielding and antibacterial	[8]

					performances	
Hhydrotherm	Bamboo	Sheet-like	Morphologies	were	Antibacterial	This
al method	power	and	modulated	by	activity and	work
		flower-like	different pH values		absorption	
		morphologies				

ACCEPTED MANUSCRIPT

Table 2 Antibacterial activity and other parameters for CNC and ZnO/CNC hybrids prepared under different pH values

Sample	$T_{5\%}^a$ (°C)	carboxyl content (mmol/g)	zeta potential (mV)	char yield (%)	ZnO content (%)	LOI^b	Antibacterial ratio	
							<i>E. coli</i> (%) ^c	<i>S. aureus</i> (%) ^c
CNC	288.2	1.13 ± 0.09	-32.4	12.4	-	22.5	-	-
ZnO/CNC8.5	267.5	0.77± 0.08	-9.9	49.5	37.1	37.3	99.6%	91.4%
ZnO/CNC10.5	312.8	0.75± 0.10	-8.9	67.4	55.0	44.5	99.7%	91.6%
ZnO/CNC11.0	312.1	0.74± 0.06	-8.5	84.1	71.7	51.1	99.8%	92.1%

^a $T_{5\%}$ was calculated from DTG curves.

^b LOI (Limiting oxygen index)= $17.5 + 0.4CR$ [13, 29, 49] (char yield evaluated at 600 °C).

^c Antibacterial ratios of *S. aureus* and *E. coli* obtained from antibacterial tests.

Table 3 Average crystallite size and crystallinity for CNC and ZnO/CNC hybrids prepared under different pH values.

Sample	Morphology, size ^a	χ_c ^b (%)	D_{200} (nm)	D_{100} (nm)	D_{002} (nm)	D_{101} (nm)
	Nanorod,					
CNC	average diameter of 10.9 nm average length of 101.7 nm	61.0	4.0	-	-	-
	Nearspherical					
ZnO/CNC8.5	average diameter of 60 nm	63.4	-	18.3	17.5	18.1
	Irregular sheet-like					
	150-500 nm in diameter					
ZnO/CNC10.5	120-790 nm in length average thickness of 10-30 nm	72.0	-	18.5	27.4	18.2
	Flower-like					
ZnO/CNC11.0	120-330 nm in diameter 840-2340 nm in length	90.1	-	16.4	28.1	16.4

^aMorphology and size were recorded from SEM micrographs.

^b χ_c was calculated from the XRD patterns

Table 4 Constants and correlation coefficients of pseudo-first order and pseudo-second order kinetic models for adsorption of MB and MG onto the ZnO/CNC hybrids.

	$q_{e,cal}(exp)$ (mg/g)	Pseudo-first-order model			Pseudo-second-order model		
		q_e (mg/g)	k_1 (min ⁻¹)	R^2	q_e (mg/g)	k_2 (gmg ⁻¹ min ⁻¹)	R^2
MB	19.672	19.5953	0.10007	0.62565	19.65989	0.05081	1
	29.28144	29.09661	0.09224	0.63501	29.25184	0.03413	0.99999
	38.95748	38.42449	0.09786	0.75521	38.70999	0.02563	0.99996
	46.77419	46.30889	0.08236	0.62218	46.62042	0.02137	0.99997
MG	19.80746	19.75934	0.10281	0.40037	19.77844	0.05047	1
	29.69919	29.56119	0.09356	0.59366	29.62674	0.03366	0.99999
	39.62891	39.56174	0.11264	0.51422	39.83367	0.02522	1
	49.51134	49.32961	0.10726	0.65027	49.6638	0.02018	1

Highlights

- ZnO/CNC nanohybrids were obtained by a green one-step synthesis technique
- Various ZnO/CNC morphologies were modulated by using bamboo CNC as biotemplate
- Nearly spherical, sheet-like and flower-like structure were modulated at various pH values
- ZnO/CNC8.5 showed superfast adsorption ability for cationic dyes within 5 min

